Analysis of Aircraft Control Strategies for Microburst Encounter

Mark L. Psiaki* and Robert F. Stengel†
Princeton University, Princeton, New Jersey

Penetration of a microburst-type windshear during takeoff or approach is an extreme harzard to aviation, but analysis has indicated that risks could be reduced by improved control strategies. Attenuation of flight-path response to microburst inputs by feedback control to elevator and to throttle was studied for a jet transport and for a general aviation aircraft using longitudinal equations of motion, root locus analysis, Bode plots of altitude response to wind inputs, and nonlinear numerical simulation. Response to several idealized microburst wind fields was studied for the approach and takeoff flight phases. Tight control of air-relative energy, pitch-up response to decreasing airspeed, increased phugoid-mode damping, and decreased phugoid natural frequency were shown to improve microburst penetration characteristics. Aircraft stall and throttle saturation were found to be limiting factors in an aircraft's ability to maintain flight path during a microburst encounter.

Nomenclature

$\bar{c}$ = mean aerodynamic chord
C_D = drag coefficient
C_L = lift coefficient
C_M = pitching moment coefficient
C_T = thrust coefficient
$E(V_a)$ = propeller efficiency factor
F = matrix coefficient of Δx in linear equations of motion (12)
g = acceleration of gravity
G = matrix coefficient of Δu in linear equations of motion (12)
h = altitude
H = total specific energy [see Eq. (17)]
H_u = matrix coefficient of Δu in linear output equation (13)
H_w = matrix coefficient of Δw in linear output equation (13)
$H_{\dot{w}}$ = matrix coefficient of $\Delta \dot{w}$ in linear output equation (13)
H_x = matrix coefficient of Δx in linear output equation (13)
I = identity matrix
I_{yy} = pitching moment of inertia
j = $\sqrt{-1}$
K = output feedback gain
L = matrix coefficient of Δw in linear equations of motion (12)
m = aircraft mass
n_z = normal load factor
P = propeller power
q = pitch rate
$\hat{q}$ = nondimensional pitch rate = $q_i \bar{c}/2V_a$
$\bar{q}$ = dynamic pressure = $\rho V_a^2/2$
r = range
r_h = horizontal extent of outflow (see Fig. 2)
r_v = horizontal extent of downdraft (see Fig. 2)
s = Laplace transform variable
S = wing reference area
t = time
T = thrust
u = control vector = $(\delta E, \delta T)^T$
V = aircraft velocity magnitude
w = wind velocity vector = $(w_v, w_h)^T$
w_h = headwind speed
w_v = downdraft speed
x = state vector = $(V_i, \gamma_i, q_i, \alpha_i, h, r)^T$
y = output vector
α = angle of attack
δE = elevator angle
δT = throttle setting
Δ = prefix signifying perturbation from nominal
γ = flight-path angle
θ = pitch angle
ρ = air density
σ = real part of complex number
τ_e = engine response time constant
ω = imaginary part of complex number
ζ_{ph} = phugoid damping ratio
$(\dot{})$ = time derivative
$(\,)_a$ = air relative
$(\,)_h$ = horizontal
$(\,)_i$ = inertial
$(\,)_0$ = nominal or trim value
$(\,)_{ss}$ = steady-state value
$(\,)_v$ = vertical

Presented as Paper 84-0238 at the AIAA 22nd Aerospace Sciences Meeting, Reno, Nev., Jan. 9-12, 1984; revision submitted July 30, 1984.

*Graduate Student, Mechanical and Aerospace Engineering.
†Professor, Mechanical and Aerospace Engineering. Associate Fellow AIAA.

Introduction

WITHIN the past ten years, several major aircraft accidents during the takeoff or approach flight phases have been attributed to a severe meteorological condition known as a microburst.[1,2] A microburst, actually a downburst of horizontal extent less than about 3 miles, is a low-altitude windshear condition consisting of a vertically descending column of air that spreads out horizontally as it hits the ground (Fig. 1). This condition is hazardous because a penetrating aircraft may first encounter a headwind that causes a pitch-up and a rise above the flight path. Then it experiences a shear of the headwind to a tailwind along with a downdraft, both of which cause it to fall below the glide path.

A recent example is the loss of a Boeing 727 aircraft during takeoff from the New Orleans International Airport in July 1982.[3] Although the aircraft's performance capability was sufficient (in theory) to allow safe penetration, a number of factors prevented this, including lack of established control procedures to be used in microburst encounter. While it is recognized that

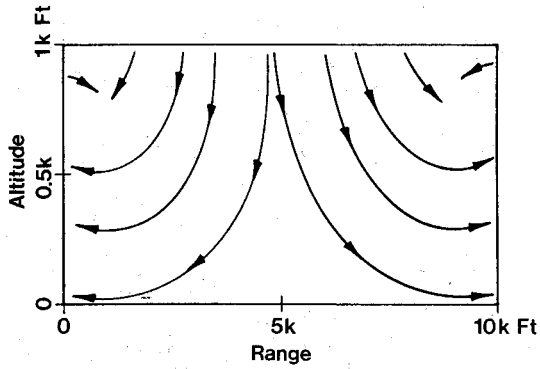

Fig. 1 Vertical cross section of a microburst wind field.

the best control strategy is total avoidance by waiting until this transient phenomenon has convected away from the airfield, optimal control strategies for inadvertent microburst penetration and the associated safe operating envelopes of typical aircraft classes remain to be determined.[4]

To date, many studies have been made of the general problem of flight through vertical shears in the horizontal wind,[5-7] and more recently attention has been given to the microburst encounter problem.[8,9] The earlier studies found the stability of the phugoid-mode to be affected by the change of the headwind (or tailwind) magnitude with altitude, dw_h/dz. A conclusion frequently reached in the flying community was that any dynamic problems associated with this windshear would be eliminated by arresting the rate of climb or descent, essentially freezing the wind speed at a constant value. Studies dealing mainly with flight through microbursts have taken the approach of simulation of microburst encounter. An extensive review of work done in this field, including microburst modeling efforts, derivations of equations of motion that include wind effects, and simulation of open-loop, piloted, and automatically controlled flight through microbursts, is given in Ref. 10. The question of proper controls for microburst penetration has also been addressed,[9,11,12] principally using linearized models of aircraft dynamics.

In this paper, the effects of various feedback control laws upon tracking of the nominal trajectory during a microburst encounter are presented. Both jet transport (JT) and general aviation (GA) aircraft are considered. This is a preliminary study of controller sensitivities based upon classical control design principles, including root loci, Bode plots of windshear response, and nonlinear simulation of microburst encounter transients. No attempt is made to address all of the issues of practical autopilot design.

Methods and Tools of Analysis

Equations of Motion

The equations of motion for symmetric flight in a variable wind field can be expressed in wind axes,[10] body axes,[9] or inertial velocity axes as presented here:

$$\dot{V}_i = \{-\bar{q}S[C_D\cos(\alpha_i-\alpha_a)+C_L\sin(\alpha_i-\alpha_a)] + T\cos\alpha_i\}/m - g\sin\gamma_i \tag{1}$$

$$\dot{\gamma}_i = \frac{(\bar{q}S[C_L\cos(\alpha_i-\alpha_a)-C_D\sin(\alpha_i-\alpha_a)]+T\sin\alpha_i}{mV_i} - \frac{g\cos\gamma_i}{V_i} \tag{2}$$

$$\dot{q}_i = \bar{q}S\bar{c}C_M/I_{yy} \tag{3}$$

$$\dot{\alpha}_i = q_i - \dot{\gamma}_i \tag{4}$$

$$\dot{h} = V_i\sin\gamma_i \tag{5}$$

$$\dot{r} = V_i\cos\gamma_i \tag{6}$$

No $\dot{\alpha}_a$ terms, other unsteady aerodynamic effects, or effects of the wind distribution over the aircraft were modeled; these are reasonable approximations in this study of the longitudinal trajectories. V_a and α_a were calculated as functions of V_i, α_i, γ_i, w_v, and w_h using the geometric transformation

$$\alpha_a = \alpha_i + \gamma_i - \tan^{-1}\left(\frac{V_i\sin\gamma_i + w_v}{V_i\cos\gamma_i + w_h}\right) \tag{7}$$

$$V_a^2 = V_i^2 + w_v^2 + w_h^2 + 2V_i(w_v\sin\gamma_i + w_h\cos\gamma_i) \tag{8}$$

Atmospheric density gradient effects were ignored, and it was assumed that the local, Earth-fixed coordinate system was inertial.

Aircraft Models

Two aircraft types were considered. The first was a three-engine jet transport in the 150,000-lb class, corresponding closely to the model in Ref. 13. The second was the single-engine, propeller-driven, general aviation aircraft described in Ref. 14.

The jet transport's lift and pitching moment coefficients were modeled as linear functions of α_a, δE, and $\hat{q}$, while the drag coefficient was a function of the squared lift. Its stall characteristics were unmodeled, but they are known to occur at about 13 deg of angle of attack. Thrust was assumed to be independent of airspeed, and there was a first-order lag between the throttle setting and the thrust,

$$\dot{T} = (\delta T - T)/\tau_e \tag{9}$$

where $\tau_e = 4$ s. Power-induced lift, drag, and pitching moment effects were not considered.

The general aviation aerodynamic model was nonlinear, being based upon full-scale wind tunnel data that include stall characteristics and power-induced lift, drag, and pitching moment effects. The aircraft's thrust was modeled as follows:

$$T = E(V_a)P/V_a \tag{10}$$

$$\dot{P} = (\delta T - P)/\tau_e \tag{11}$$

The first-order throttle-response time constant was 1 s.

Microburst Description

The meteorological phenomenon of microbursts is currently the subject of an extensive experimental study,[15] and better models are being developed for flight simulation.[16,17] The models used for this study, however, were only rough approximations, as in Ref. 10. The vertical and horizontal wind velocities were modeled as functions of range along the flight path. Two microburst shapes were considered. The first involved discrete steps in horizontal wind and downdraft. The second had the headwind varying to a tailwind as one period of a sine wave, while the downdraft varied as one period of a $[1-\cos(2\pi r/r_v)]$ transient (Fig. 2).

As can be seen, these simplified models retain the essential dangers to flight: a headwind shearing to a tailwind accompanied by a downdraft. Therefore, they can reveal major features of the aircraft trajectory response. In reality, the wind profiles experienced during penetration will depend upon the trajectory and upon the shape, period, and intensity of the microburst.[18] The discrete microburst model excited short-period response at the step edges, but was otherwise similar to the sinusoidal model. The trajectory differences were minimal, so the remainder of this paper reports results only for the sine-wave microburst model. Several wavelengths and amplitudes were considered; for this study, the nominal

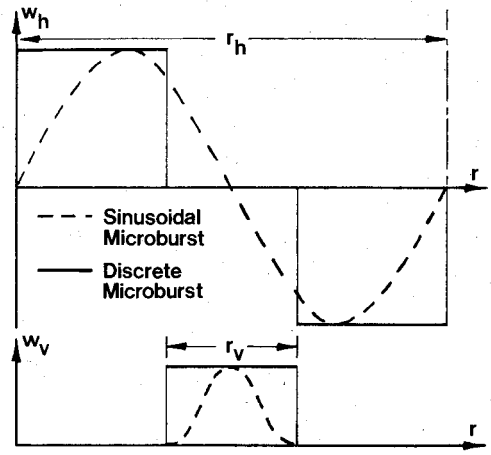

Fig. 2 Simplified microburst models, dependence of w_h and w_v on r.

Table 1 Nominal trim conditions for two aircraft

	JT	GA
V_i, ft/s	235	110
γ_i, deg	−3	−3
α_i, deg	3.6	6.2
δE, deg	−3.1	−6.1
δT, % of max	40	24

microburst was taken to be $r_h = 10{,}000$ ft, $w_h(\max) = 35$ ft/s for the headwind-to-tailwind wave and $r_v = 3{,}000$ ft, $w_v(\max) = 20$ ft/s for the downdraft. The nominal wavelengths and amplitudes correspond roughly to the windshear reported for a 1976 accident at Philadelphia International Airport.[9]

Flight Phase

This paper concentrates primarily upon the approach flight phase, where the aircraft is nominally trimmed at constant airspeed and flight-path angle. Nominal trim conditions for the two aircraft are listed in Table 1. An example of the steady climb-out flight phase also is considered, with nominal $\gamma_i = 3$ deg. Neither landing flare nor liftoff and rotation are addressed, and aerodynamic ground effects are ignored.

Control Law Design, Analysis, and Simulation

Linearized equations of motion were derived from Eq. (1-11) for perturbations from trim. The dynamic equation takes the form:

$$\Delta\dot{x} = F\Delta x + G\Delta u + L\Delta w \tag{12}$$

The output equation can be expressed as

$$\Delta y = H_x\Delta x + H_u\Delta u + H_w\Delta w + H_{\dot{w}}\Delta\dot{w} \tag{13}$$

The following elements of Δy were considered for feedback control law formulation: V_a, α_a, $\bar{q}\alpha_a$, θ_i, γ_i, H_a, $\dot{H}_a$, H_i, $\dot{H}_i$, and h. Control laws of the form $\Delta u = -K\Delta y$ were examined for stability by means of classical root locus plots.

The control laws were next examined in terms of Bode plots of closed-loop transfer functions from time-dependent wind inputs, Δw, to state outputs such as Δh. The transfer function matrices were generated according to the following formula:

$$\frac{\Delta x(s)}{\Delta w(s)} = [sI - F + G(I + KH_u)^{-1}KH_x]^{-1}$$
$$\times [L - G(I + KH_u)^{-1}K(H_w + sH_{\dot{w}})] \tag{14}$$

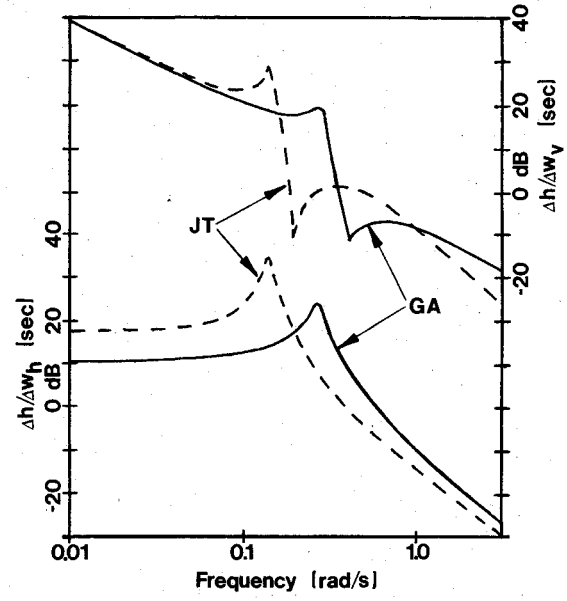

Fig. 3 Open-loop (OL) Bode gain plots for two disturbance transfer functions and two aircraft.

To evaluate microburst frequency content, an approximate transformation based upon the aircraft's nominal trajectory is used to go from spatially dependent to time dependent wind fields:

$$\Delta w(t) = \{w_v[r_0(t)], w_h[r_0(t)]\}^T \tag{15}$$

where

$$r_0(t) = tV_{i_0}\cos\gamma_{i_0} \tag{16}$$

Although the assumed microburst profiles provided transient inputs, they possessed identifiable characteristic periods. It was found that closed-loop amplitude response at the corresponding frequencies was a good predictor for the transient response obtained in nonlinear simulation.

Finally, control designs were verified using the full nonlinear equations of motion in conjunction with a fourth-order Runge-Kutta numerical integration to simulate the aircraft response. Stability was verified, and transient response to various microbursts was studied. Transient response was evaluated primarily in terms of trajectory tracking performance: h vs r plots, with attention given to angle-of-attack excursions as regards stall and to control saturation, the most significant nonlinearities of the system.

Results and Discussion

Open-Loop System Performance

As a point for comparison, the open-loop response for each aircraft model was studied using two Bode plots, the altitude response to horizontal wind input $\Delta h(s)/\Delta w_h(s)$, and the altitude response to vertical wind input $\Delta h(s)/\Delta w_v(s)$ (Fig. 3), and using the simulated transient response for several microbursts (Fig. 4).

Some features of the Bode plots can be explained as follows. The high resonant peaks are due to the light damping of the phugoid mode. The phugoid period is approximately proportional to airspeed; hence, the GA model has a higher natural frequency. GA model propeller effects cause higher phugoid damping; hence, the peaks are broader. The $\Delta h(s)/\Delta w_v(s)$ amplitude responses have −20 dB/decade slope at low frequency because the vertical velocity of an aircraft at equilibrium with respect to an air mass depends directly upon the vertical velocity of the air mass. The amplitude of both $\Delta h(s)/\Delta w_h(s)$ curves at low frequency can be explained by

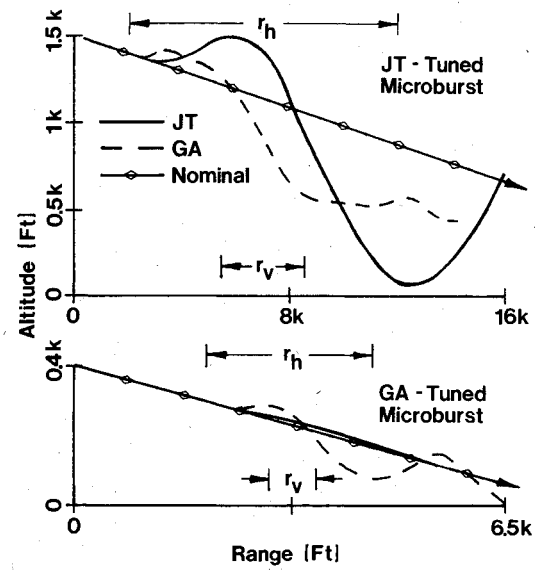

Fig. 4 Transient response trajectories for two open-loop aircraft and two microbursts.

considering conservation of total air-relative energy. If an aircraft crossed a boundary between a calm zone and a steady headwind zone, it would experience a step increment in total air-relative energy because of the step increment in airspeed, while there would be no instantaneous change in altitude. With controls fixed, the aircraft would settle back to its original airspeed after the transient had died out. To within order ζ_{ph}, the total air-relative energy would be the same as when it first entered the headwind zone. Therefore, the final altitude must be higher. Given:

$$H_a = h + V_a^2/2g \tag{17}$$

Taking the derivative of (17) to find the linear approximation for small perturbations yields:

$$\Delta H_a = \Delta h + (V_0/g)\Delta V_a \tag{18}$$

The specific energy perturbation is initially due only to the increase in airspeed, $\Delta V_a = \Delta w_h$:

$$\Delta H_{a_0} = (V_0/g)\Delta w_h \tag{19}$$

while the steady-state perturbation is due entirely to altitude increase:

$$\Delta H_{a_{ss}} = \Delta h \tag{20}$$

Combining Eqs. (19) and (20) yields

$$\frac{\Delta h}{\Delta w_h} = \frac{V_0}{g} \tag{21}$$

a value that depends only upon nominal airspeed and which correesponds closely to the low-frequency limits on the Bode plots. This result would not hold in the true steady state if atmospheric density gradient effects were considered.

It could be expected that a microburst head/tailwind period in the vicinity of the aircraft's phugoid period would produce a resonant response, while the aircraft altitude should respond to the downdraft portion of the microburst by integrating the $[1-\cos(2\pi r/r_v)]$ pulse. In fact, the nominal microburst chosen in this paper is well tuned to the JT aircraft model considered here (not surprising in light of the Philadelphia accident), so the controls-fixed transient response to this microburst was simulated for both aircraft. Also simulated for

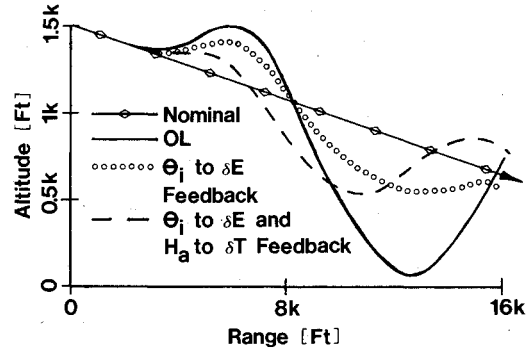

Fig. 5 Comparison of closed-loop (CL) transient responses to nominal microburst.

the controls-fixed case was the response to a GA-tuned microburst with a period of 2500 ft. For this case, the peak winds were one-quarter of the nominal values to maintain the same maximum wind gradient. The simulated trajectories for these two cases appear in Fig. 4 along with the nominal flight path.

As expected, the responses for the tuned cases look like phugoid oscillations with altitude drops superimposed during the downdraft sections. Similar jet transport results were presented by Frost.[10] The Bode plots predict the response magnitudes remarkably well for the untuned cases: GA aircraft in a JT-tuned microburst and JT aircraft in a GA-tuned microburst. For the tuned cases, however, the response is lower than predicted by the linear models. This probably is due to the transient nature of the simulation vs the steady-state nature of the Bode plot results, and/or to the fact that the time frequencies of excitation and of the aircraft phugoid modes vary with the actual inertial velocity. The Bode plots predicted the relative magnitudes of the various responses, and they prove to be useful tools for the prediction of microburst attenuation by feedback control.

Of further note is that the GA response to the JT-tuned microburst resembled the tracking by a low-pass filter of a signal within its response bandwidth. The JT response to the GA-tuned microburst, on the other hand, was very low, as expected in the case of a low-pass filter being excited at frequencies above its bandwidth.

Closed-Loop-System Design and Test

For discussion, closed-loop analysis focuses on the jet transport, and the significant differences for the GA model are then noted. A good closed-loop system must do three things to decrease the effects of windshear upon the flight path:

1) Eliminate the resonant peak in the altitude response to horizontal windshear at the phugoid natural frequency.

2) Eliminate the integration effect in the altitude response to downdraft.

3) Lower the altitude response to horizontal windshear at all frequencies below the phugoid.

The first goal can be achieved simply by adding damping to the phugoid mode. Pitch angle or flight-path angle feedback to the elevator is known to do this. With moderate gains, a damping ratio of $\zeta_{ph} = 0.7$ can be achieved, eliminating the resonant peak altogether. The corresponding trajectory responses to the nominal microburst are almost identical for the two control laws, so only the one for the θ_i-to-δE control law is shown in Fig. 5.

This closed-loop trajectory now looks somewhat like the open-loop trajectory for the GA aircraft in this same microburst. The response magnitude indicated by the Bode plot corresponds closely to that observed in the simulation. The response is, of course, still unacceptable: Deviations from

the glide slope reach several hundred feet, but a significant improvement has been made.

The second goal—elimination of the intergration effect of the downdraft upon the steady-state altitude response—is somewhat less easily achieved. Clearly, some inertial quantity such as altitude deviation Δh must be fed back. A feedback quantity like h has been considered for windshear applications[11]: total air-relative specific energy. One reason for interest in this quantity is the existence of an inexpensive $\dot{H}_a$ sensor.[19] Using a method similar to Ref. 7 of studying the closed-loop stability as affected by dw_h/dz, it can be shown that H_a-plus-$\dot{H}_a$-to-δT feedback restabilizes the phugoid mode when dw_h/dz destabilizes it.[11] This feedback also stabilizes the altitude mode, so it is a candidate for achieving the second goal.

First consider the root locus for H_a feedback to δT in Fig. 6. Although the rigid-body longitudinal motion of the aircraft plus the engine dynamics and altitude feedback yield a sixth-order system, Fig. 6 resembles the root locus of a second-order system. This is because total specific energy varies little with phugoid or short-period oscillations. Therefore they are almost unobservable in H_a, and their eigenvalues cannot be greatly affected by feedback of H_a to δT. Consequently, the altitude-mode pole can be placed independently of the phugoid and short-period poles by using H_a feedback to δT. Closing this loop leads to the Bode plots of altitude response to downdraft, $\Delta h(s)/\Delta w_v(s)$, shown in Fig. 7.

The desired elimination of the integration effect upon the steady state has been achieved. Of course, the phugoid mode damping still must be increased to eliminate the resonant peak. This can still be done, for example, by θ_i feedback to δE without adversely affecting the new result. For this multiple-loop case, the trajectory from the simulated transient response to the nominal microburst appears in Fig. 5.

The nonlinear transient response trajectory shows a larger maximum deviation than for the case of θ_i feedback to the elevator alone. The additon of the H_a-to-δT loop improved the performance in the headwind zone, and it eliminated much of the final bias due to the downdraft; however, it resulted in a larger deviation from the glide path in the tailwind zone. From the Bode plots, one would have expected the horizontal-shear-induced phugoid oscillations to be about the same as for the case of θ_i feedback to the elevator, with the downdraft-induced bias being eliminated to yield a better net result. The throttle time history explains this discrepancy. One finds that the throttle setting was reduced in the headwind zone, then increased quickly to saturation in the downdraft and tailwind zones. The Bode plot for the throttle setting response to horizontal wind input, $\Delta\delta T(s)/\Delta w_h(s)$, likewise predicts that 150% of maximum throttle was required by this controller to negotiate this windshear. The trajectory response was not as predicted by the Bode plots because of the nonlinear effect of throttle saturation. It was worse than for the case of θ_i feedback to the elevator because throttling back during the headwind zone caused a loss of energy that could not be made up quickly enough during the downdraft-tailwind zone when the throttle saturated.

Even if throttle saturation had not been a problem in this case, the $\Delta h(s)/\Delta w_h(s)$ frequency response was still too high near the phugoid natural frequency. The maximum deviation from the nominal flight path still would have been on the order of hundreds of feet for the microburst considerd. In other words, the third design goal still must be achieved.

One way to accomplish this is to increase the gain in the H_a-to-δT feedback loop, but this presents two problems: δT saturation will occur for even lower wind inputs, and the damping ratio of the combined altitude-engine mode will be decreased. In order to solve the second problem, $\dot{H}_a$ feedback to δT can be added such that the new zero on the root locus falls just to the left of the pole associated with the engine dynamics. The resulting root locus is plotted in Fig. 6.

This allows an increase in the gain without decreasing the damping ratio. As regards the saturation problem, one would expect the addition of this loop to exacerbate it. Actually, the addition of this loop allows for an increase in gains while slightly decreasing throttle activity at frequencies up to the phugoid. At frequencies above the phugoid, the problem will get worse, but throttle activity is not needed at high frequency because the open-loop system response is acceptable in that range. Even when the throttle saturates, one can see that this feedback loop will perform better than H_a-to-δT feedback alone because it will respond more rapidly with full throttle to the altitude loss in the downdraft zone and the airspeed loss in the tailwind zone.

Another feedback loop that showed some promise of lowering the altitude response to horizontal wind input near the phugoid natural frequency was $\bar{q}\alpha_a$ to δE. In simple aerodynamic theory, $\bar{q}\alpha_a$ is approximately proportional to normal load factor, so all results that were derived for this case would be roughly the same if the feedback were from n_z to δE. Plotting the phugoid portion of the root locus indicates that this loop closure destabilizes the phugoid; however, by adding a proportional feedback of γ_i to δE, the phugoid can be stabilized (Fig. 8). γ_i is roughly proportional to the integral of $\bar{q}\alpha_a$, so this is like a proportional-integral control law.

Combining this elevator control law with the H_a-plus-$\dot{H}_a$-to-δT control law yields the Bode plots of Fig. 9 and the simulated trajectory response to the nominal microburst of Fig. 10. The lowering of the low-frequency end of the $\Delta h(s)/\Delta w_h(s)$ Bode plot was due partly to the addition of the $\dot{H}_a$-to-δT feedback loop, but it was due primarily to the use of

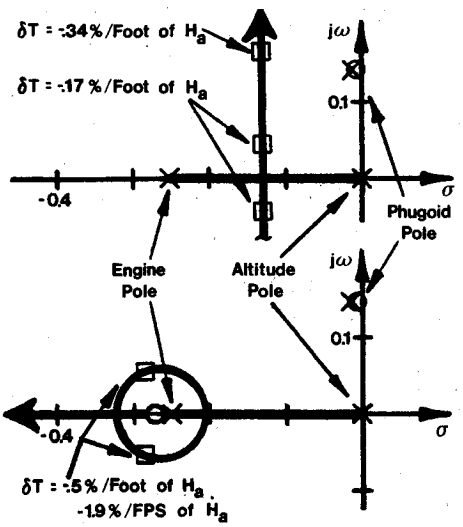

Fig. 6 Phugoid portions of two root loci. Top: H_a to δT; bottom: H_a plus $\dot{H}_a$ to δT.

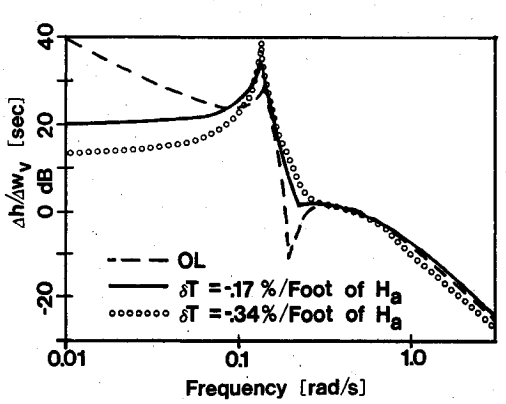

Fig. 7 Comparison of closed-loop Bode gain plots for a disturbance transfer function.

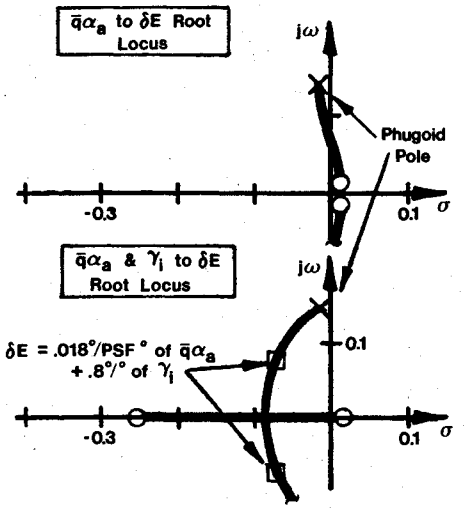

Fig. 8 Phugoid portions of two root loci.

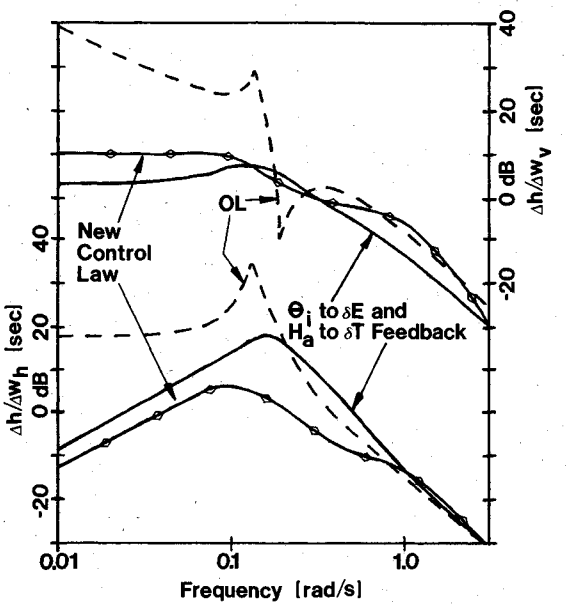

Fig. 9 Comparison of closed-loop Bode gain plots for two disturbance transfer functions.

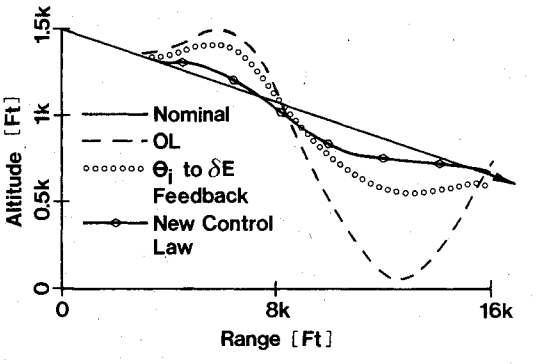

Fig. 10 Comparison of closed-loop transient responses to nominal microburst.

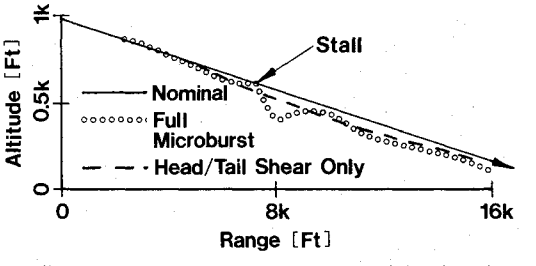

Fig. 11 Closed-loop transient response of GA aircraft to two microbursts.

H_a in the throttle feedback loop. The lowering of the peak in the $\Delta h(s)/\Delta w_h(s)$ Bode plot was due to the lowering of the phugoid natural frequency that resulted from the $\bar{q}\alpha_a$-plus-γ_i-to-δE feedback. Nonlinear transient response is improved by this control law, but it is not as good as the Bode plots would indicate, again because of throttle saturation. For the reason given earlier, the addition of $\dot{H}_a$ feedback improved the response, even though throttle saturation occurred.

Another reason for the improved performance of this feedback control law was that it responded to a decrease in airspeed (or $\bar{q}$) by pitching up. This concept is the reverse of what a pilot normally would do, but it may be essential for improved performance during microburst penetration. On the root locus, it was shown that this type of feedback tends to lower the phugoid natural frequency (Fig. 8). On the Bode plots, it was seen that a lowered phugoid natural frequency translated into a lower maximum altitude response to horizontal windshear (Fig. 9). One might consider lowering the phugoid natural frequency even further to attenuate the peak response even more. The gain from $\bar{q}\alpha_a$ to δE starts becoming very large, and the stability of the system becomes more sensitive to this gain. This represents a definite limitation to the approach.

Other feedback quantities were tried, including V_a, α_a, h, H_i, and $\dot{H}_i$. V_a showed promise in the linear analysis when fed back to δE in the opposite sense from usual. In this case, it behaved like $\bar{q}\alpha_a$, but this loop proved to be highly sensitive to gain variations that could cause the closed-loop system to diverge in a "tuck" mode. Feedback of α_a to δE in a destabilizing direction provided improved microburst penetration performance by lowering the phugoid natural frequency, effectively detuning the aircraft from the microburst, but this control law is otherwise unacceptable. Feedback of altitude caused stability problems in connection with δE, and it had too much lag to be effective by itself in actuation of δT. Inertial specific energy and energy rate were less effective feedback variables than their air-relative counterparts; the Bode plots did not have the desired properties, and transient response was degraded. This occurs because the forces and moments that provide trajectory control and disturbance response are aerodynamic.

General Aviation Case

The results for the GA model were similar to those for the jet transport, although feedback gain values were not the same. One major difference was for the control law feeding $\bar{q}\alpha_a$ and γ_i back to δE and feeding H_a and $\dot{H}_a$ back to δT: The aircraft stalled during the downdraft portion of the nominal microburst. This shows the ultimate limitation of any control law that responds to a decrease in airspeed with an increase in angle-of-attack. When the same control law was used and the downdraft portion of the microburst was omitted, the results were very good (Fig. 11), so the GA aircraft has more difficulty with the downdraft than with the outflow. A simulation of the GA aircraft with the above described control law in the GA-tuned microburst showed good performance improvement.

Climbout Case: Jet Transport Model

Simulations of climbout for the JT model through the nominal microburst were run for the open-loop case and for the $\bar{q}\alpha_a$-plus-γ_i-to-δE and H_a-plus$+\dot{H}_a$-to-δT feedback control case. The trajectories are plotted in Fig. 12. The closed-loop response is not as well attenuated as in the approach case

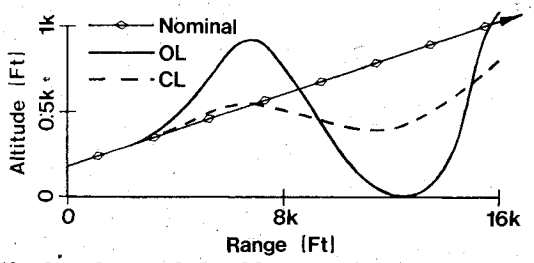

Fig. 12 Open-loop and closed-loop transient response to nominal microburst, climb-out case.

because the throttle setting is nominally 82% of the maximum; therefore throttle saturation occurs earlier, allowing a large deviation below the nominal flight path.

Conclusions

This paper brings to light several important aspects of microburst penetration by aircraft during landing or takeoff. The root loci and Bode plots of linear system analysis are useful for the design of microburst-insensitive control laws, but nonlinearities such as throttle saturation and aerodynamic stall characteristics play important parts in limiting microburst penetration capabilities. Therefore, simulation of the nonlinear equations of motion is essential in studying this problem. Tight regulation of energy with respect to the air mass can improve microburst penetration characteristics. Control laws that respond to decreasing airspeed with a pitch-up command perform better than those that do not, provided the aircraft does not stall. This characteristic was linked to the lowering of the phugoid natural fequency as a means of microburst response attenuation. Implementation of a simple gain-type feedback control law using this idea is not suggested because of aircraft stall characteristics and because of possible "tuck" mode excitation due to gain sensitivity. Although attention was restricted to elevator and throttle control, consideration should be given to the use of fast-acting, direct-lift devices such as partially deflected spoilers and flaps as well.

Acknowledgments

This research was supported in part by the National Aeronautics and Space Aministration and the Federal Aviation Administration under Grant No. NGL 31-001-252. M.L. Psiaki is supported by a National Science Foundation Graduate Fellowship.

References

[1]Fujita, T.T., "Downbursts and Microbursts—An Aviation Hazard," *Proceedings for the 19th Conference on Radar Meteorology,* April 1980, Miami, Fla., American Meteorological Society, 1980, pp. 94-101.

[2]"Aviation Weather," U.S. Congressional Hearing, Aug. 11, 1982.

[3]"Pan American World Airways, Inc., Clipper 759, Boeing 727-235, N4737, New Orleans International Airport Kenner, Louisiana, July 9, 1982," National Transportation Safety Board, Washington, D.C., Aircraft Accident Report 83/02, March 1983.

[4]Townsend, J., ed., "Low-Altitude Wind Shear and its Hazard to Aviation," National Research Council, Washington, D.C., Sept. 1983.

[5]Etkin, B., *Dynamics of Atmospheric Flight,* J. Wiley & Sons, New York, 1972, pp. 378-384.

[6]Sherman, W.L., "A Theoretical Analysis of Airplane Longitudinal Stability and Control as Affected by Wind Shear," NASA TN D-8496, July 1977.

[7]Gera, J., "The Influence of Vertical Wind Gradients on the Longitudinal Motion of Airplanes," NASA TN D-6430, Sept. 1971.

[8]Frost, W. and Crosby, B., "Investigations of Simulated Aircraft Flight Through Thunderstorm Outflows," NASA CR 3052, Sept. 1978.

[9]Rynaski, E.G. and Govindaraj, K.S., "Control Concepts for the Alleviation of Windshears and Gusts," NASA CR 166022, July 1982.

[10]Frost, W., "Flight in Low-Level Wind Shear," NASA CR 3678, March 1983.

[11]Gera, J., "Longitudinal Stability and Control in Wind Shear With Energy Height Rate Feedback," NASA TM 81828, Nov. 1980.

[12]Lehman, J.M., Heffley, R.K., and Clement, W.F., "Simulation and Analysis of Wind Shear Hazard," Federal Aviation Administration, Washington, D.C., RD-78-7, Dec. 1977.

[13]Turkel, B.S. and Frost, W., "Pilot-Aircraft System Response to Wind Shear," NASA CR 3342, Nov. 1980.

[14]Shivers, J.P., Fink, M.P., and Ware, G.M., "Full-Scale Wind Tunnel Investigation of the Static Longitudinal and Lateral Characteristics of a Light, Single-Engine, Low-Wing Airplane," NASA TN-D-5857, June 1970.

[15]McCarthy, J., "The Joint Airport Weather Studies Project—Current Analysis Highlights in the Aviation Safety Context," AIAA Paper 84-0111, Jan. 1984.

[16]Zhu, S. and Etkin, B., "Fluid-Dynamic Model of a Downburst," University of Toronto, Toronto, Canada, UTIAS Rept. 271, Feb. 1983.

[17]Bray, R.S., "Windshear Modeling for Simulation," NASA Ames Research Center presentation to the Panel on Aircraft Performance and Operations, Commitee on Low-Altitude Wind Shear and Its Hazard to Aviation, National Research Council, at NASA Langley Research Center, Hampton, Va., May 25, 1983.

[18]Frost, W. and Chang, H.P., "Simulated Flight Through JAWS Wind Shear: In-Depth Analysis Results," AIAA Paper 84-0276, Jan. 1984.

[19]Nicks, O.W., "A Simple Total Energy Sensor," NASA TM X-73928, March 1976.